Chapter

Modeling of a Contact-Less Electric-Vehicle Battery-Charging Station Fed from On-Grid Photovoltic Arrays

Essamudin Ali Ebrahim

Abstract

Electric vehicles (EVs) are environmental friendly due to no exhaust gases or carbon dioxide. In addition, there is no noise through operation. However, up to now, there are some challenges that facing its spread through all over the world. The main problem that these vehicles face is the fast charging process of the used batteries through neat and clean source without plugs. So, this chapter deals with a proposed method for a contactless battery charger of both electric and hybrid electric vehicles (HEVs) from renewable resources. The chapter proposes a public station for fast charging. This station implies off-board battery charger fed from on-grid (OG) photovoltaic (PV) arrays through inductively power transfer (IPT). This comfortable 100 kW contactless power station is designed, modeled, and simulated as a general software package reliable to be used for any other station design. The air gap of the air-core transformer (ACT) divides the station into two parts. The first part implies roof-mounted PV array with its intelligent-controlled maximum power point tracking (MPPT) technique, power converter, three-level power inverter, and resonant compensator converter that operates at high frequency. The second one includes rectifiers and switched mode power converter with smart controller. The chapter includes samples for simulation results that are obtained from the Matlab software package.

Keywords: contactless power transfer, inductive power transfer (IPT), air-core power transformer (ACPT), electric vehicle (EV), photovoltaic (PV), three-level inverter

1. Introduction

Several research works have been introduced to contribute toward introducing an environmentally friendly power source to replace the conventional internal combustion engine (ICE). Electric vehicles (EVs) and fuel cell electric vehicles (FCEVs) expected to be replaced soon. It is known that the EVs have higher efficiency for the energy conversion, capability for regenerative braking and motoring, minimum emission for exhaust gases, and low noise and vibration when compared with ICEs.

The host battery, its total cost, and the development of its performance play an important role in the electric vehicle (EV) and hybrid EV [1]. The battery charging process needs several considerations such as fastness, safety, easy, and low-priced cost.

There are two techniques for charging process: plug-in and un-plugged but connected. Out-door plug-in needs to have a large cable that creates power losses, inconvenience, and electric-chock hazards for most owners. But, on the other hand, inductively coupled power transfer (ICPT) contactless-charging system introduces an imperious solution for the risk and embarrassment problems through transferring the charging energy over a softly inductive coupler [2–4].

Through the last decade, several aspects of ICPT have been studied, such as magnetic coupler design techniques, compensation topologies, control methods, foreign object detection algorithms, and the radiation safety issues [5–7]. Also, the main power supply for the station prefers to be renewable and friend to the environment. High-rating good quality and low-priced photovoltaic (PV) cells – as a renewable energy supply – are nowadays available and suitable to this purpose [8]. Several efforts for progressing the ICPT charging technique are done as described by Miskovski and Williamson [9]. The authors suggested that a 100-kW public solar power station – with battery banks – for partial charging (30%) only and 10% of the required power is supplied from the PV array. The main disadvantages of that system are that it uses a battery bank with bulky and expensive elements for the public-charging station. Also, in Ref. [10], the author presented a charge controller of solar photovoltaic panel (SPV) fed battery. But in [11], Robalino et al. suggested a solar energized docking charging with fuel cell for electric vehicle. The study proposed an alternative method for manufactures and consumers to use the clean sources for transportation commitments. This study has limited theoretical guides for the designers to model the station.

However, this chapter introduces a study that came to provide an integrated model for a solar-powered electric vehicle charging station connected to the main grid. This chapter introduces a complete modeling and designing for a public station of electric vehicle battery charging with a wireless technique. This technique depends on inductively coupled power transfer (ICPT) by using air-core transformer (ACT) to overcome the problems of contacts and wiring due to high-rating charging current. The proposed station is fed from a renewable power resource such as PV arrays connected with the main grid. The study includes the design for the PV array with its maximum power point tracking (MPPT) and its mathematical model. Also, this chapter introduces a Matlab/m-file software package that includes a model for boost converter required for interconnecting between PV array and load with its smart control. In addition, the package introduces a complete design and model for three-level inverter interconnecting between the PV and the main grid. This chapter also proposes an air-core transformer with light weight and a few number of turns for inductively coupling. The proposed system utilizes a buck converter for battery charger to control the charging current with an intelligent PI-tuning controller. In addition, a high-frequency resonant converter with series compensation is modeled and simulated through this study. The validity of the system is verified by charging four 19-kW lithium-ion batteries of Honda EV in order to test the capacity and efficiency of the station.

2. The proposed ICPT-PV for EV public-charging station

The proposed public-charging station consists of two main parts (as shown in **Figure 1**): the static and dynamic sections. The rated power of the station is 100 kW, and it depends on the types and capacity of the EV batteries to be charged.

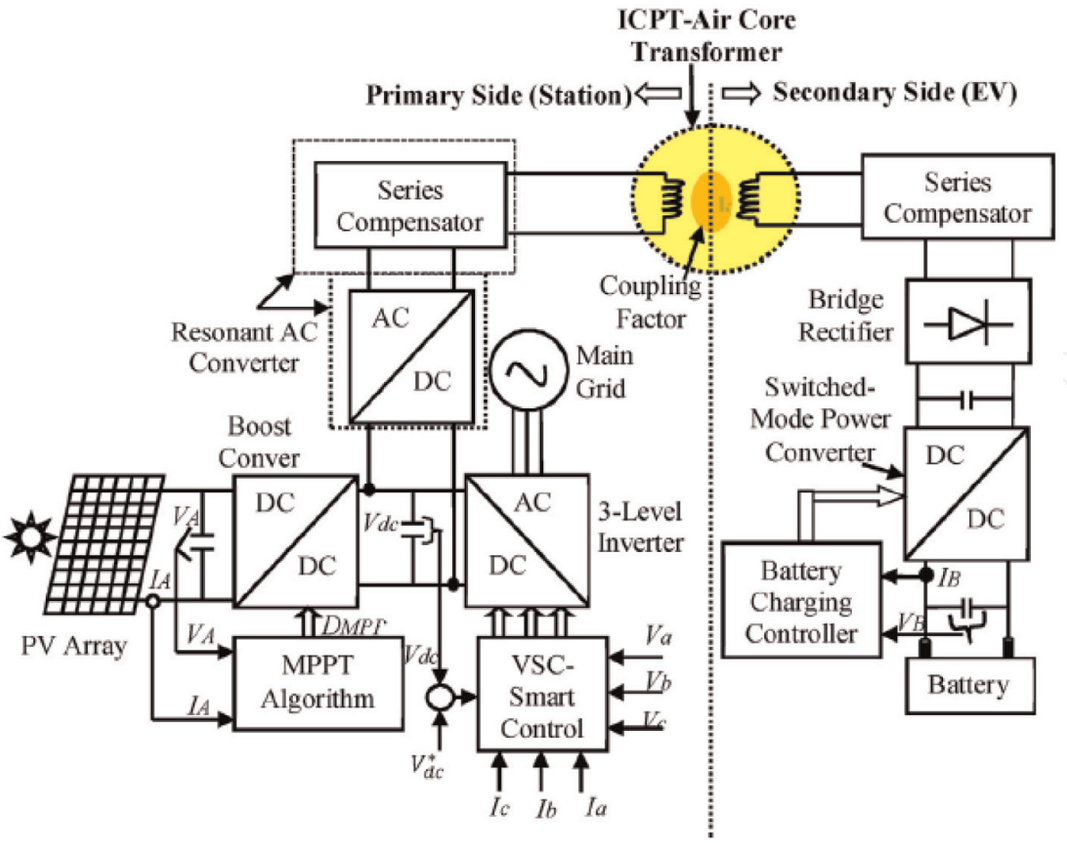

Figure 1.
The proposed public station for PV battery charging.

The average capacity for most batteries used in electric vehicles is around 20 kWh. The parts of the station are classified according to the position that is placed. Static part is the part that placed on land or under ground in the station. But, the dynamic part is that placed inside the EV as on-board battery charging. Each part of the station will be explained and designed in detail in the following sections.

3. The primary-side part

The primary-side part consists of the modeled PV panels in arrays as a neat-renewable energy source with its controller for the maximum power point tracking (MPPT) that implies one boost converter, a bi-directional three-level inverter for interfacing with the main grid and the PV arrays, and resonant converter with very high frequency including a series compensator, and all are connected with the air-core transformer (ACT) through its primary winding.

3.1 Modeling of the PV array with MPPT algorithm

The PV cell, module, and arrays mathematical models can be obtained by Essamudin [8] according to the following equations:

The total current of the cell is computed as follows:

$$I = I_{irr} - I_o\left[e^{\left(\frac{q(V+IR_s)}{nkT}\right)} - 1\right] - \frac{V + IR_s}{R_p} \tag{1}$$

Also, the total current of the module can be computed from the following equation:

$$I_M = I_{irr} - I_o\left[e^{\left(\frac{q\left(V_M + I_M N_s R_s\right)}{N_s nkT}\right)} - 1\right] - \frac{V_M + I_M N_s R_s}{N_s R_p} \tag{2}$$

Then, the total PV array current is given by the following criteria:

$$I_A = N_p I_{irr} - I_o\left[e^{\left(\frac{q\left(V_A + I_A \frac{N}{N_p} R_s\right)}{N_s nkT}\right)} - 1\right] - \frac{V_A + I_A\left(\frac{N}{N_p}\right)R_s}{\frac{N_s}{N_p}R_p} \tag{3}$$

where I, I_M, I_A are the cell, module, and array currents (A); I_{irr} is the irradiance or photo current (A); I_o is the diode saturation current (A); V, V_M, V_A are the cell, module, and array voltages (V); $q = 1.6 \times 10^{-19}$ (C); $K = Boltizmann\ constant = 1.3806503 \times 10^{-23}$J/K; R_s, R_p are series and parallel resistance (Ω); N_s, N_p are series and parallel cell numbers; and T is the cell temperature (°K).

The proposed station is designed to work as on-grid with 100-kW power rating supplied from the PV source in the day light (not using battery banks as storage elements), and it will be supplied from the main grid in the evening and cloud days. So, the following lines show the modeling and designing for the number of PV modules with arrays to generate the power needed.

The rated power for the station is 100 Kw, and the rated output voltage for the PV array is 300 V, if it is supposed that the SunPower module (SPR-305) types [12–14] are used with their characteristics: voltage for open circuit (V_{oc}) is 64.2 V, current for short circuit (I_{sc}) is 5.96 A, maximum power voltage and current V_{MPP} is 54.7 V and I_{MPP} is 5.58 A, $\therefore N_s = \left(\frac{300}{64.2}\right) = 4.6 \cong 5$ modules, then the DC output terminal voltage of the PV array will be 320 V.

If the maximum power for one module equals $(54.7 \times 5.58) \cong 305\ W$, then the total required number of modules can be obtained as $\left(\frac{100000}{305}\right) = 327$ modules = $N_s \times N_p$; dependently, if the total numbers of the parallel modules are calculated as $(327/5) \cong 66$ modules, then the total required modules for the proposed system are $(66 \times 5 = 330)$, and the maximum power will be equal to P_{MPP}=(330×305)/1000 = 100.65 kW.

When the dimension of one proposed module is 1.559m × 1.046m = 1.63m^2 [14], then, the total surface area required is equal ($1.63 \times 330 \cong 538$m^2). This area can be saved on the station roof and used to arrange the modules in rows and columns. However, the characteristic curves of one module and one array for the V-I and V-P curves are illustrated in **Figure 2 (a** and **b)**, respectively.

3.2 Maximum power point tracking (MPPT) algorithm with boost converter

There are several methods proposed to achieve MPPT [15, 16]. The simplest method is the incremental conductance (IC) that depends on the base that the maximum power point is obtained when the power slope of the PV is zero that obtained from the derivative of the power due to the voltage and equating it to zero (i.e., $dP/dV = 0$). **Figure 2a** and **b** describes this and explores the characteristic curves of both power and current with the PV terminal voltage of one module and one array. As shown, the left side of the curve is positive and negative in the right. Due to this condition, the MPP can be found in terms of the increment in the array conductance. In Eq. (4), if the value of the error in the right hand side equal zero, this means that the change of current due to voltage equal to negative value of the

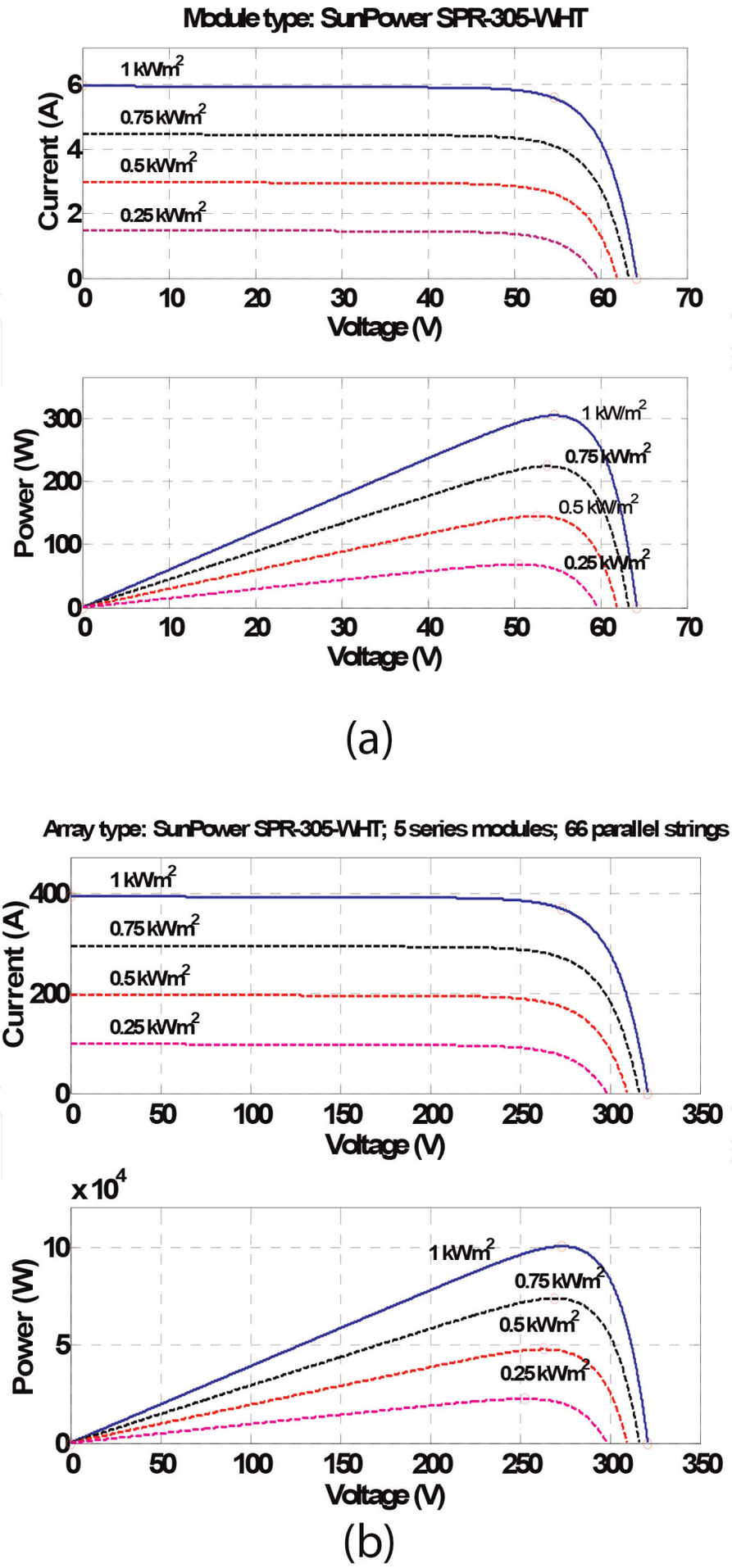

Figure 2.
V-I and V-P characteristics for (a) one module and (b) the PV array.

division of current by voltage. The quotient of this division equal to the incremental conductance (IC).

$$\frac{dP_A}{dV_A} = \frac{d(V_A.I_A)}{dV_A} = I_A + V_A \frac{dI_A}{dV_A} = \text{error} \tag{4}$$

The IC has three states that can be presented by the following Eqs. From Eq. (5)–(7) [15].

$$\frac{\Delta I_A}{\Delta V_A} = -\frac{I_A}{V_A} = -G \tag{5}$$

or

$$\frac{\Delta I_A}{\Delta V_A} > -\frac{I_A}{V_A} \tag{6}$$

or

$$\frac{\Delta I_A}{\Delta V_A} < -\frac{I_A}{V_A} \tag{7}$$

At MPP, the right-hand side (RHS) of the equation equals to the left-hand side (LHS; Eq. 5). If the LHS is greater than RHS (Eq. 6), the power point lies on the left. If Eq. (7) is verified, the point lies in the right of MPP. This method is similar to the Perturb and Observe method for searching the MPPT. This method has good power transient performances through the atmospheric conditions rapid changes.

The error signal (e) can be minimized by using an integral regulator, then the duty ratio at MPP (D_{MPP}) is obtained as:

$$D_{MPP} = K_I \int_0^{\Delta t} \left(\frac{\Delta I_A}{\Delta V_A} + \frac{I_A}{V_A} \right) dt \tag{8}$$

The final output control signal needed to trigger the IGBT boost converter switch can be obtained with the help of Matlab/Simulink as illustrated in **Figure 3**.

3.3 Boost converter

The main function of boost converter is used to boost voltage, so it is used with PV to raise its output voltage from 320 to 540 V. The main components are a series inductor with shunt capacitor, and both are controlled through the electronic

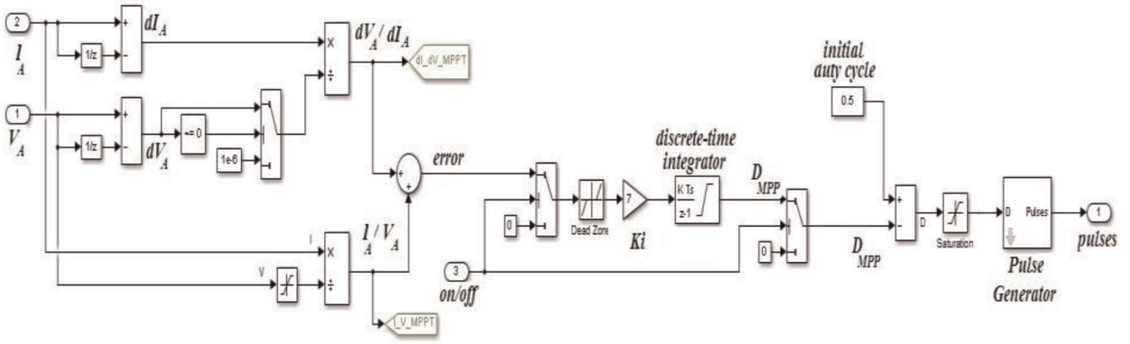

Figure 3.
Matlab/Simulink MPPT algorithm with boost-converter pulse generation.

switches such as MOSFET or IGBT (as shown in **Figure 4**). The main triggering signals are generated as train of pulses from MPPT-algorithm output when the duty-ratio varies.

3.4 Soft-switching multi-level three-phase diode-clamped inverter topology

The three-phase multi-level (with three-level) diode-clamped inverter that proposed in this research is shown in **Figure 5**. The main idea depends on the topology of the neutral point clamped (NPC), which was proposed by Nabae, Takahashi, and Akagi in 1981 [17, 18].

To interconnect between the DC output of the PV and the main AC-grid, it should be used as a bi-directional converter to transfer power from DC-side to AC-one and vice versa. So, a three-level voltage-source current-controlled converter with neutral point clamped (NPC) is proposed. **Figure 5** shows the circuit configuration of the NPC inverter. Each leg has four IGBTs connected in series. The applied voltage on the IGBT is one-half of the conventional two-level inverter. The bus voltage is split into two by the connection of equal series connected bus capacitors. Each leg is completed with the addition of two clamp diodes. The main advantages of this technique are its capability of handling higher voltages, lower line-to-line and common-mode voltage steps, and lower output current ripple for the same switching frequency as that used in a two-level inverter.

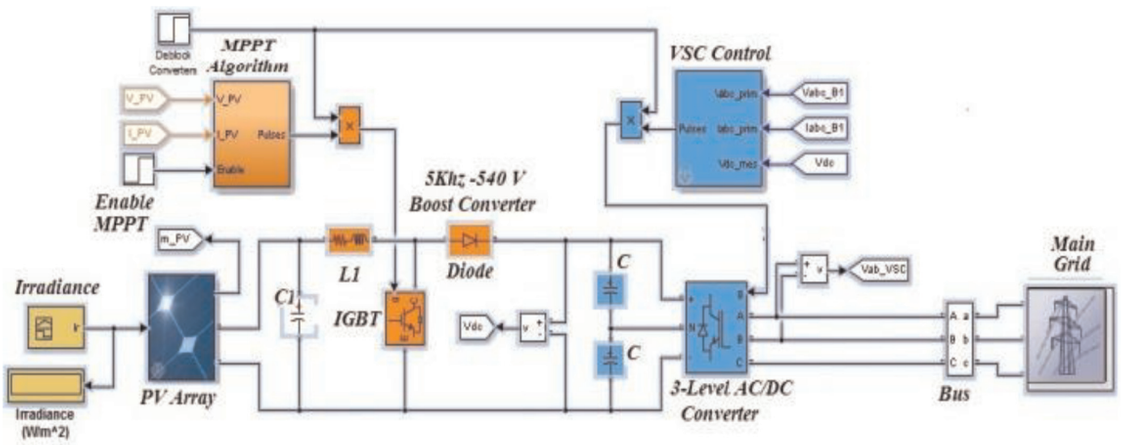

Figure 4.
Modeling of on-grid PV array with MPPT converter and inverter set.

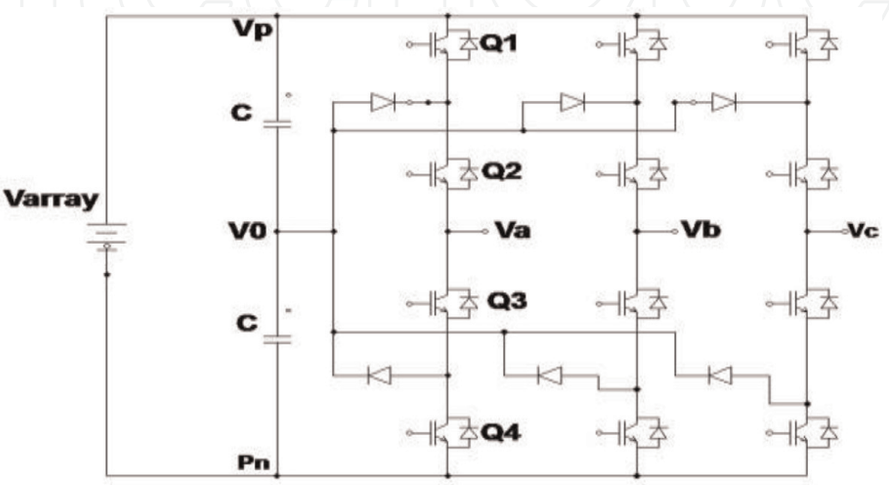

Figure 5.
Three-phase three-level inverter (power circuit).

This converter can produce three voltage levels on the output: the DC bus plus voltage (V_p), zero voltage (V_0), and DC bus negative voltage. For a one phase (phase A) operation, when IGBTs Q_1 and Q_2 are turned on, the output is connected to V_p; when Q_2 and Q_3 are turned on, the output is connected to V_0; and when Q_3 and Q_4 are turned on, the output is connected to V_n [19].

3.5 Voltage-source DC/AC converter/inverter control

The boost-converter output should be constant and equal or greater than the peak value of the AC supply voltage for the grid. To do this, a robust controller should be used. The proposed technique uses PI-smart controller with self-tuning adaptive (K_p, K_i) parameters by using bacteria-foraging optimization algorithm (BFO). The voltage error signal e_v is the difference between the actual and reference DC-link voltage $\left(e_v = V_{dc}^* - V_{dc}\right)$. This value should be minimized to a small or zero [8]. The DC-link voltage can be computed as the value that equals to peak value of the line-to-line voltage ($380\sqrt{2} \cong 540$ V). In the same time, the inverter power factor (P.F.) is equal to unity. This can be achieved by using another PI-smart controller for the current and making $I_{qs}^* = 0$. This controller is used to minimize the current error signal that is the difference between the direct reference and the actual current components $\left(e_i = I_{ds}^* - I_{ds}\right)$. **Figure 6** illustrates the overall control algorithm and the Matlab/Simulink blocks. The switching frequency for the converter is equal to 30 KHz to give 50 Hz voltage output.

3.6 Modeling of contactless power-transfer air-core transformer (ACT)

One of the more reliable and safe ways to transfer power is un-pugged but connected wireless method. This method depends on the inductively coupling air-core transformer with a large air gap. The power is energized from the floor of the station to the primary winding, and then by the effect of induction, it is transferred to the secondary winding that puts under the vehicle through a wide air gap. So, this transformer needs special construction to design the primary and secondary windings and its air-gap. There are several configurations for this transformer such as the core of coil: some have air core, and others have iron core. Also, several factors should be taken into consideration through modeling and designing of ACT such as

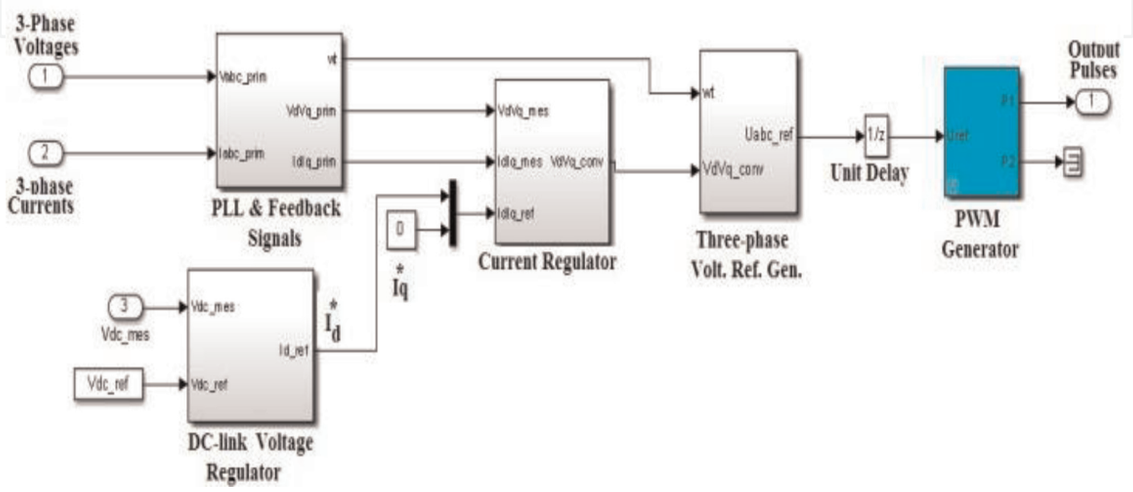

Figure 6.
Control algorithms for DC-link voltage and current regulator for three-level inverter.

the air gap between the primary and secondary winding, cost of the magnetic material for the core, weight of the core, eddy current losses in the core, operating frequency, and sensitivity to misalignment between primary and secondary windings. Due to the large air gap for the transformer, this configuration leads to a large leakage inductance and low mutual coupling that involves a large magnetizing current. Because of CPT transformer with air core has a lightweight with core losses, it is selected in this study for both windings. The coupling coefficient, k, affects directly on the capability of the power transferred of the ICPT. This coefficient can be computed as $k = \frac{M}{\sqrt{L_1 L_2}}$, where L_1 and L_2 are the self-inductance coefficients of the primary and secondary coils, and M is the mutual inductance between them. **Figure 7a** shows the schematic diagram of the transformer, and **Figure 7b** illustrates the equivalent circuit of the model, where L_p and L_s are the leakage inductance of both primary and secondary windings of the ACT. The power-transfer capability to the batteries can be improved by compensation to eliminate the effect of induction. This can be achieved by connecting a capacitor in both sides of the transformer. It is called series-series (SS) compensation as shown in **Figure 7c**. This combination makes the primary capacitance independent of both

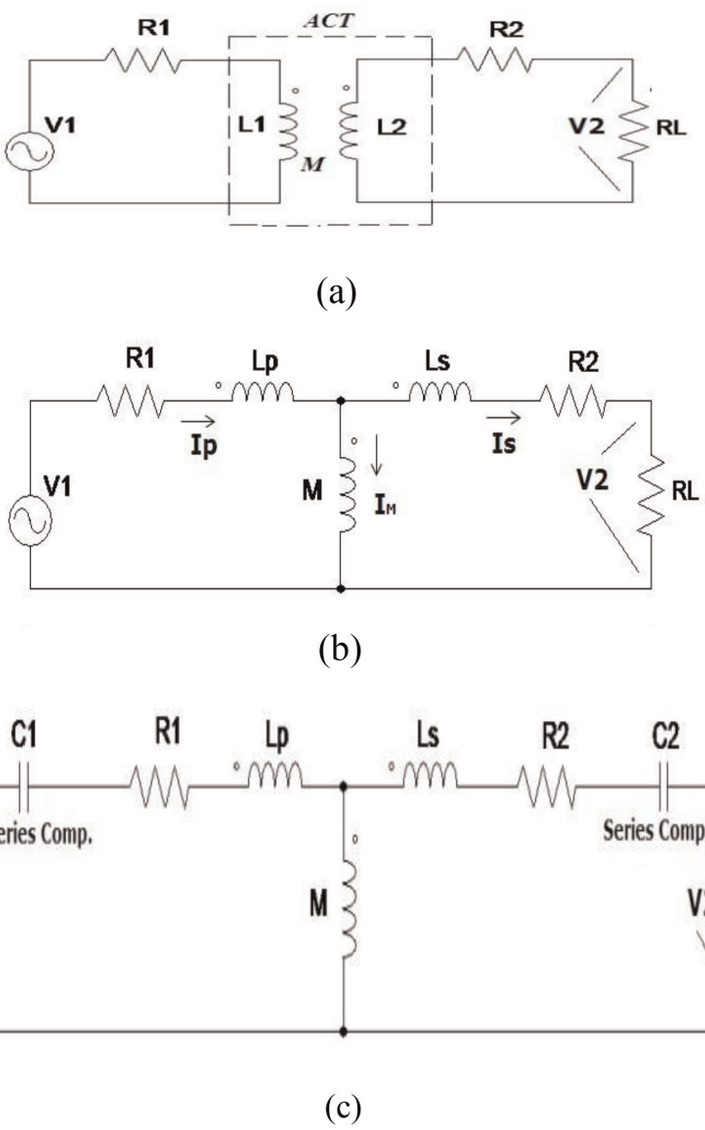

Figure 7.
Modeling of an ICPT air-core transformer with SS compensation. (a) Schematic diagram. (b) Equivalent circuit. (c) Equivalent circuit with SS-compensation.

the magnetic coupling and the load [2]. According to the resonant frequency through both primary and secondary coils, it can compute and select the values of the primary and secondary capacitances C_1 and C_2, respectively. This maximizes the power transferred to the batteries and improves the power factor of the supply to unity.

The power transferred from the primary to the secondary is given as follows:

$$P_2 = \frac{\omega_0^2}{R_L} M^2 I_p^2 \tag{9}$$

where ω_0, I_p, and R_L are the resonant frequency, primary current, and the load resistance, respectively. The value of ω_0 is chosen equal to both primary and secondary windings and can be computed as follows:

$$\omega_0 = \frac{1}{\sqrt{L_p C_1}} = \frac{1}{\sqrt{L_s C_2}} \tag{10}$$

So, the capacitance values of both primary and secondary windings $C_1$and C_2 can be obtained as follows:

$$C_1 = \frac{1}{L_p \omega_0^2} \text{ and } C_2 = \frac{1}{L_s \omega_0^2} \tag{11}$$

Designing of ACT depends on the values of its parameters L_1, L_2, and M. This can be obtained from its physical dimensions. The coils with rectangular form are proposed to both primary and secondary windings of ACT (as shown in **Figure 8**). The advantage of this form is giving much better tolerance to misalignment. The flow chart illustrated in [4] illustrates the design process for the overall ACT, and the parameters of 100 kW charging station are tabulated in **Table 1**.

A general software package with help of the Matlab m-file is introduced for designing and simulation of the ACT. This package is validated with much accuracy for any ACT with a rectangular form for different dimensions and relative position between them.

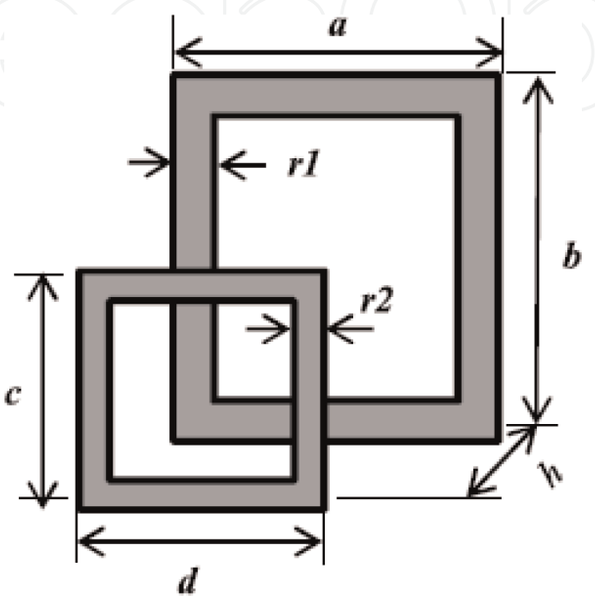

Figure 8.
Geometrical dimensions of the proposed ACT.

Parameter	Value
No. of primary turns (N_1)	6
No. of secondary turns (N_2)	4
Radius of the primary coil (r_1)	9.27 mm
Radius of the secondary coil (r_2)	8.00 mm
The primary-coil length and width *(a,b)*	0.9 m
The secondary-coil length and width *(c,d)*	0.6 m
Internal resistance of the primary (R_1)	1.2365 mΩ
Internal resistance of the secondary (R_2)	2.2781 mΩ
Primary self-inductance (L_1)	0.082 mH
Secondary self-inductance (L_2)	0.041 mH
Mutual inductance between coils (M)	.011 mH
Air gap length	175 mm
The coupling coefficient, k	0.2
Voltage of secondary (V_2)	500 V
Resonant frequency (f_0)	20 KHz
Power of secondary (P_2)	100 kW
Primary series compensation (C_1)	0.7722 uf
Secondary series compensation (C_2)	1.5441 uf

Table 1.
Parameters of ACT.

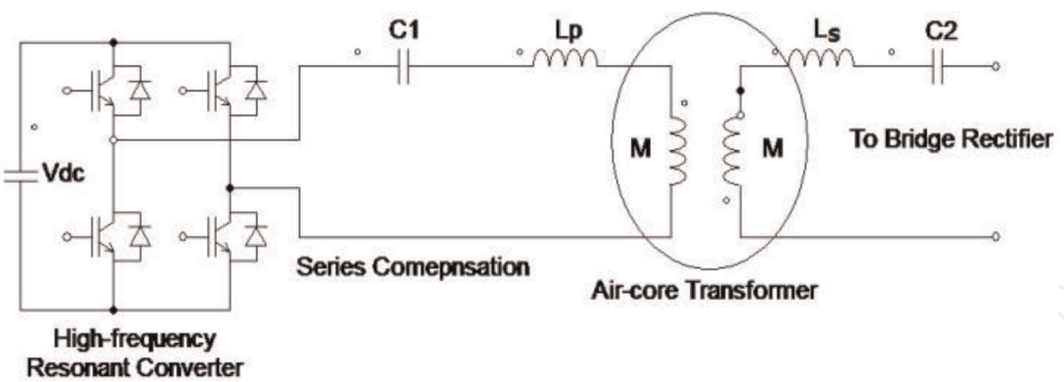

Figure 9.
The high-frequency resonant converter with SS compensation of ACT.

3.7 Resonant DC/AC high-frequency converter

DC-link output voltage cannot be transferred directly to the AC transformer. So, a resonant AC converter is required. This converter is a single-phase bridge inverter switched at a very high-resonant frequency as shown in **Figure 9**. The output of the converter is fed to the primary winding of the air-core transformer through a series compensated capacitor.

4. Second part (mobile side)

The second part of the proposed system implies the secondary coil of the ACT that constructed inside the EV with inductive coupling with primary winding

through the air gap. This side (as shown in **Figures 1** and **10**) includes single-phase uncontrolled bridge rectifier, switched-mode power buck converter with its intelligent battery-charging controller, and tracking batteries.

4.1 DC/DC Buck converter

An un-controlled bridge rectifier is required to convert the energized AC secondary-coil power to a DC current. The output voltage of the bridge is greater than the battery-terminal voltage. So, a buck converter (as shown in **Figure 10**) is needed. The main components of it are a controlled switch, diode, series reactor, and shunt capacitor. The proposed smart control circuit is proposed to adapt the battery-bank charging voltage (**Figure 11**).

4.2 Mathematical model of EV battery

The actual mathematical dynamic model of EV battery for simulation will be obtained from Refs. [20, 21] in the following sections:

4.2.1 For lead-acid battery

Charging:

$$V_{bat} = E_0 - R.i - K\frac{Qi^*}{(it - 0.1\,Q)} - K\frac{Qit}{(\,Q - it)} + e^t \tag{12}$$

$$\text{Discharge}: V_{bat} = E_0 - R.i - K\frac{Q(it + i^*)}{(\,Q - i.t)} + e^t \tag{13}$$

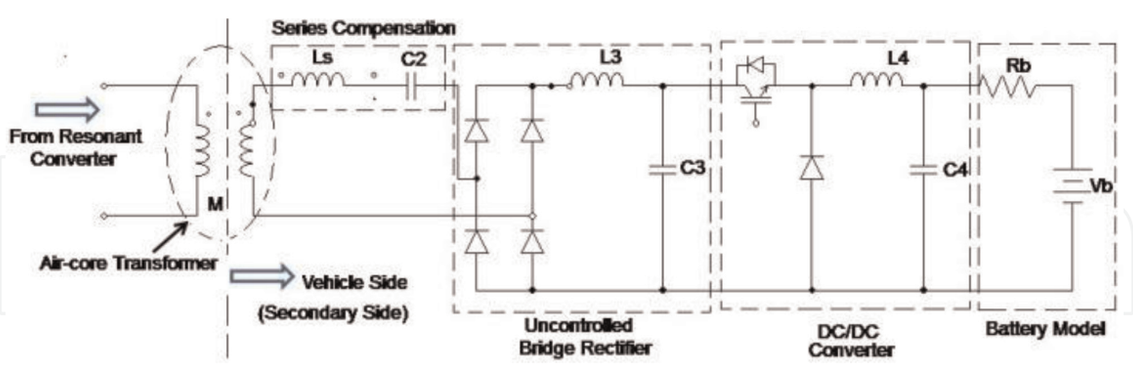

Figure 10.
Components of the electric vehicle section (secondary side).

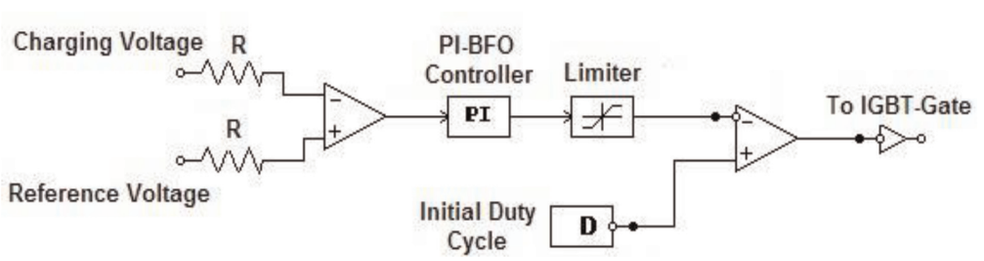

Figure 11.
The control circuit of Buck converter.

4.2.2 Li-ion battery

Charging:

$$V_{bat} = E_0 - R.i - K\frac{Qi^*}{(it - 0.1\,Q)} - K\frac{Qit}{(\,Q - it)} + Ae^{-B.it} \tag{14}$$

Discharge:

$$V_{bat} = E_0 - R.i - K\frac{Q(it + i^*)}{(\,Q - it)} + Ae^{-B.it} \tag{15}$$

4.2.3 NiMH and NiCd battery

Charging:

$$V_{bat} = E_0 - R.i - K\frac{Qi^*}{(|it| - 0.1\,Q)} - K\frac{Q.it}{(\,Q - it)} + e^t \tag{16}$$

$$\text{Discharge}: V_{bat} = E_0 - R.i - K\frac{Q(it + i^*)}{(\,Q - it)} + e^t \tag{17}$$

where V_{bat} is the voltage of the battery (V), E_0 is the battery constant voltage battery (V), K is the constant of polarization ($V = Ah$) or resistance of polarization (Ω), Q is the capacitance of the battery (Ah), $it = \int idt$ is the actual charge of the battery (Ah), R is the internal resistance of the battery (Ω), i is the current of the battery (A), i^* is the current of battery filtered (A), A is the amplitude of exponential zone (V), and B is the time-constant inverse of the exponential zone $(Ah)^{-1}$.

5. Simulation results and discussion

A Matlab/Simulink and m-file general software package are introduced for designing 100-kW EV-battery charger of a renewable-energized public station. The data obtained in Section 3 are used to build the PV arrays. The given parameters from **Table 1** are also used to simulate the ACT transformer needed for the ICPT. The ACT HV windings are proposed to be made from the twisted Litz conductors to minimize the eddy losses [1].

To test the proposed charging system, four 19-Kwh identical EV Honda batteries are charged at the same time. The charging voltage rate is 200 V. When the state of charging (SOC) reaches to 30%, the battery starts to charge. The proposed simulated data for the IGBT-rated voltage and current are 1500 V and 200 A, respectively. To test the robustness of the system against PV fluctuation, the PV-irradiance profile is assumed to vary in the range of 1000 and 250 W/m^2 as shown in **Figure 12a**. Dependently, the PV output terminal voltages with and without using the proposed smart controller are illustrated in **Figures 12b** and **e**, respectively.

The duty ratio of the converter with time according to the variation of irradiance and terminal voltage is shown in **Figure 12c**. The power profile with irradiance variation is clearly illustrated in **Figure 12d**. Through time interval 0.5–0.7, the irradiance reduced from 1000 to 250, and dependently, the power also reduced from 100 kW to less than 20 kW.

This illustrates the importance of the on-grid technique for the station. The modulation-index profile of the three-level interconnected inverter is illustrated in

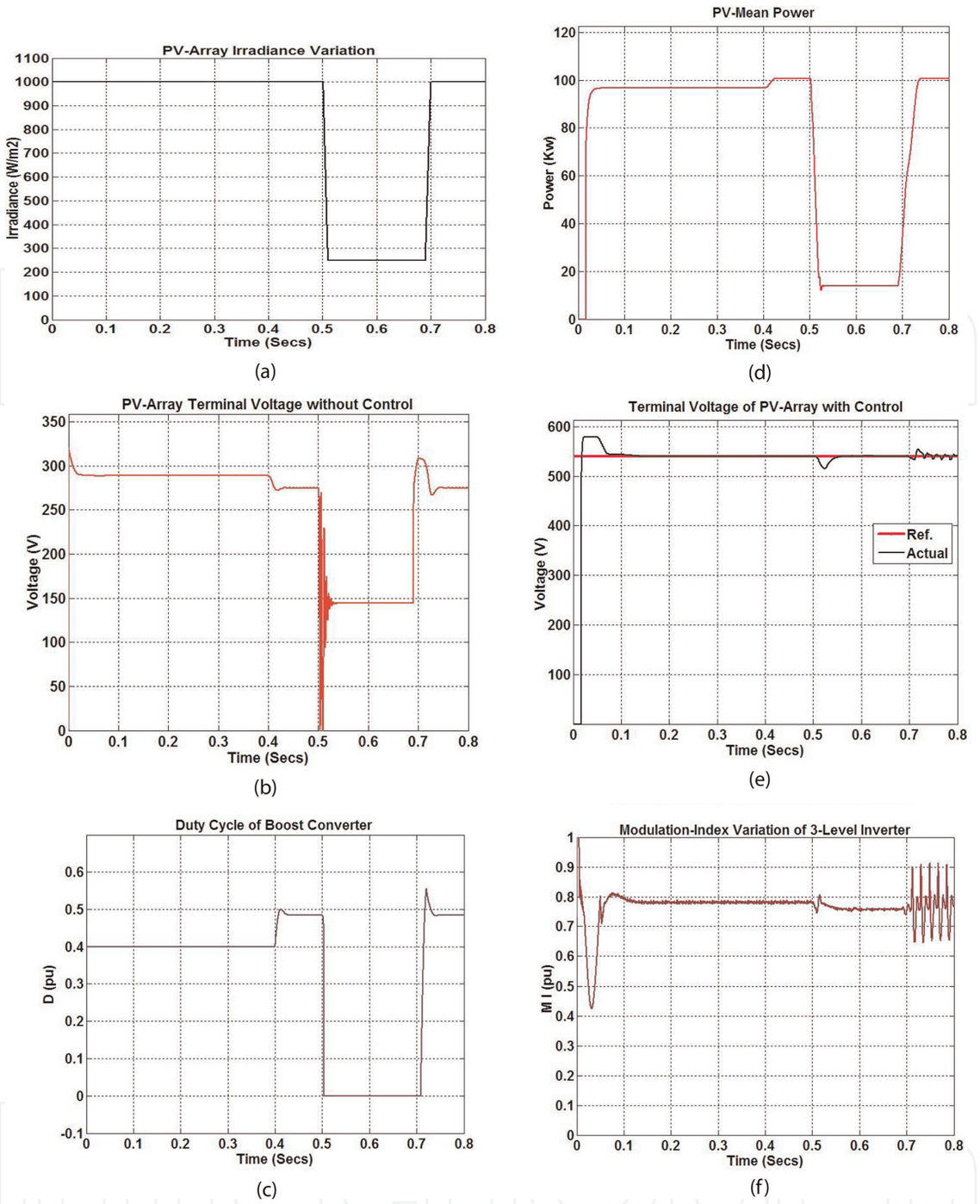

Figure 12.
(a) PV-array irradiance. (b) PV-array terminal voltage profile. (c) Duty cycle for boost converter. (d) PV mean power. (e) PV-array terminal voltage (reference and actual). (f) Modulation-index variation of three-level inverter.

Figure 12f. The figures illustrate the inverter output-voltage changes with the variation of PV irradiance.

Dependently, **Figure 13** shows a comparison for both the 3-level line to line output voltage of the inverter and the grid. It can be noticed that the line voltage maximum value of both is about 540 V ($380\sqrt{2}$). **Figure 14** illustrates the resonant converter output voltage with its high-frequency value that is equals to 30 KHz.

So, both **Figures 15** and **16** describe the high-frequency input voltage and current of the ACT-primary winding, respectively. On the other hand, the voltage and currents of the secondary winding of ACT are illustrated in both **Figures 17** and **18**, respectively.

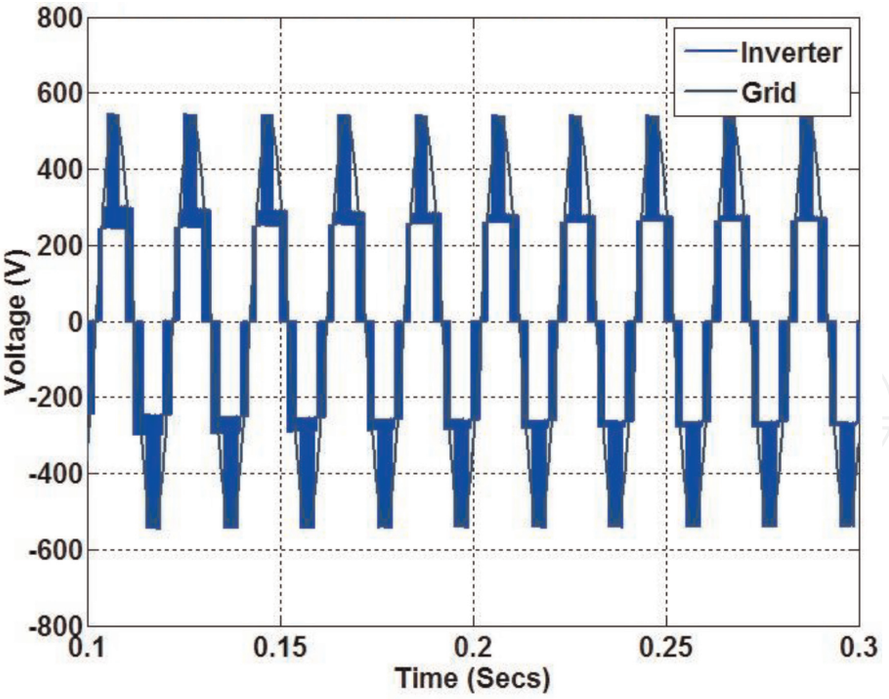

Figure 13.
Line voltage of both three-level inverter and the main grid.

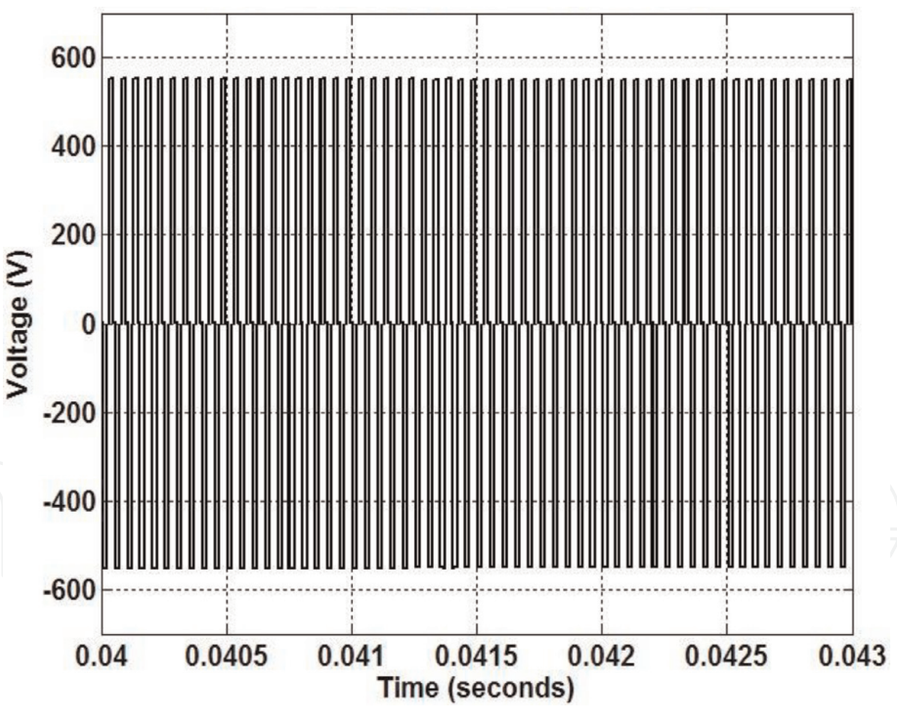

Figure 14.
High-frequency inverter-output voltage.

By using ACT with its turns ratio equal (10:6), when the primary voltage equals to 1000 V, the secondary-winding output voltage equals to 600 V. **Figure 19** describes the simulation results for the initial battery state of charge (SOC) that equals to 30%.

The EV-Honda battery-charging current profile with time is shown in **Figure 20**. According to switching process of the buck converter, the current varies according to the signals of current controller.

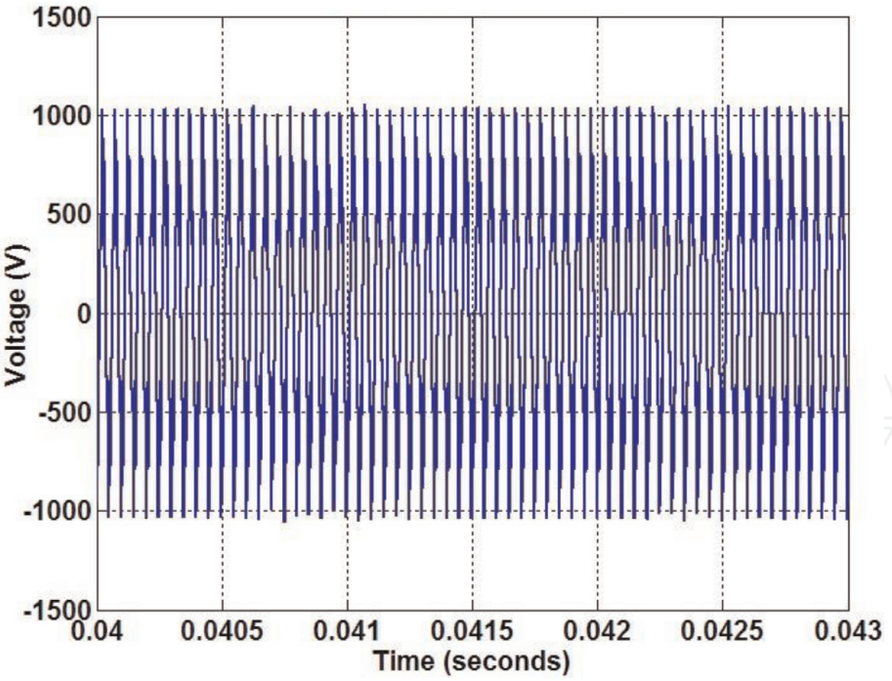

Figure 15.
ACT-primary voltage.

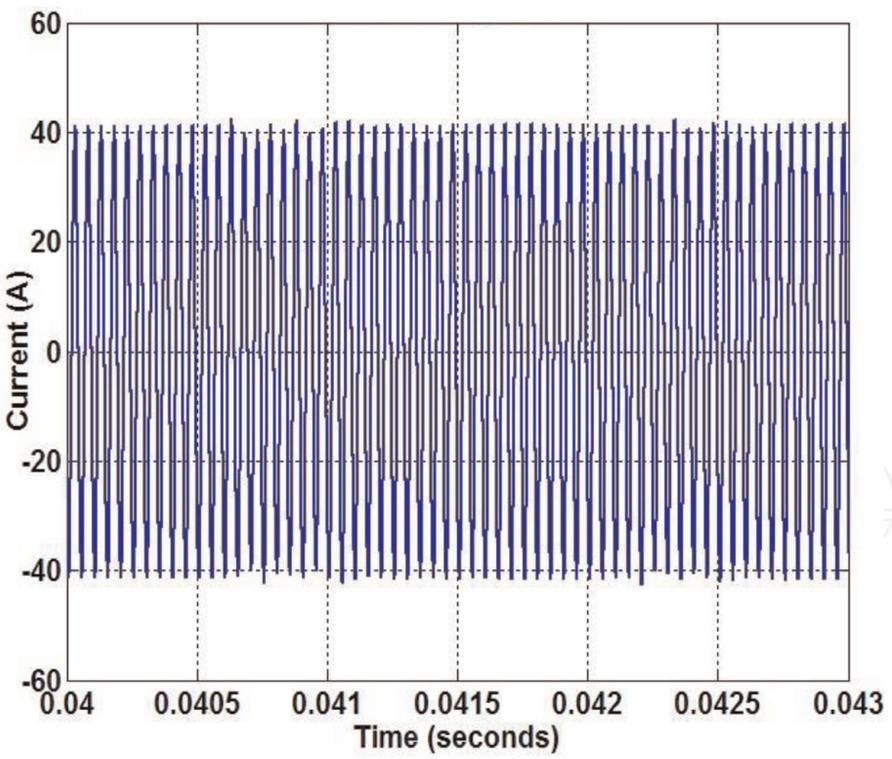

Figure 16.
ACT-primary current.

Also, the voltage level through battery-charging process is demonstrated in **Figure 21**. The value of the battery voltage is controlled to be kept constant, where the charging process is achieved at constant voltage.

However, the overall average charging efficiency can be calculated as follows:

$$\eta_{ol} = \left(\frac{P_o}{P_i} \times 100\right) = \left(\frac{nv_b i_b}{P_m} \times 100\right) = \left(\frac{4 \times 200 \times 90}{94000}\right) \cong 76.6\% \tag{18}$$

where v_b and i_b are the voltage and current (V,A) of the battery charging, respectively; n is the number of batteries to be charged; and P_m is the PV average power (W).

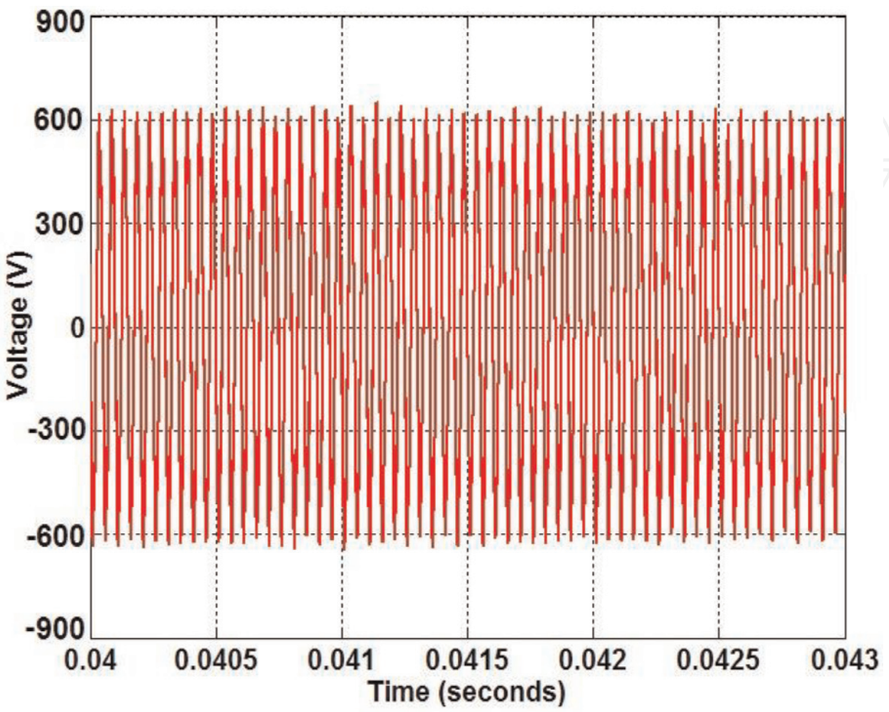

Figure 17.
ACT-secondary voltage.

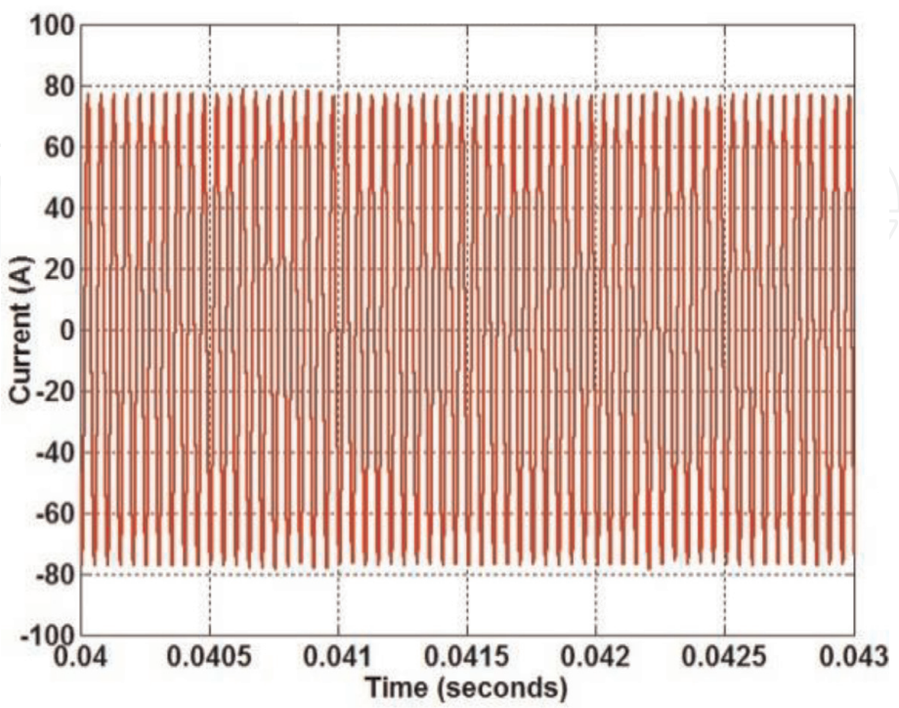

Figure 18.
ACT-secondary current.

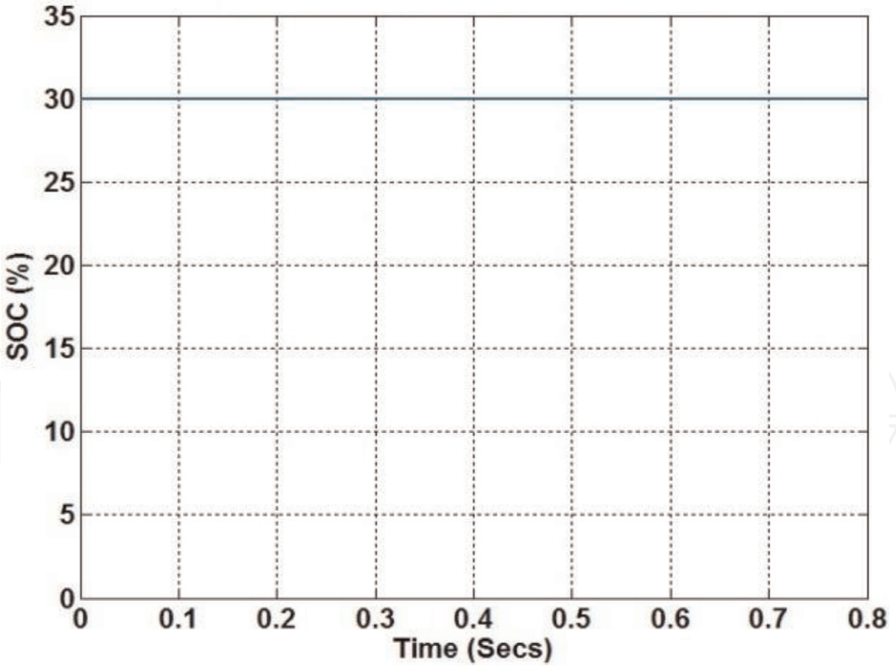

Figure 19.
Initial-battery state of charge (SOC).

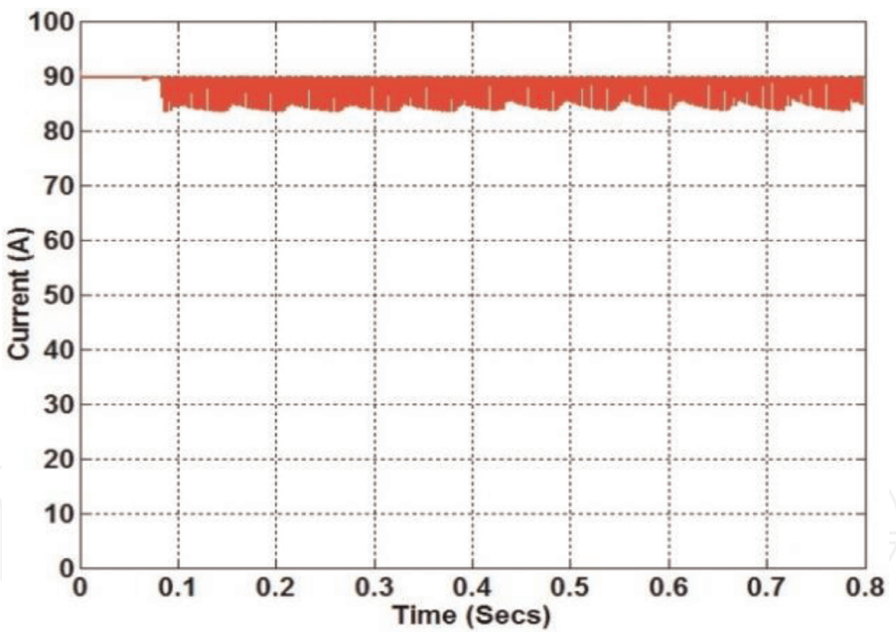

Figure 20.
Battery-charging current.

It should be noted that the efficiency calculated above is the approximate value because of using ideal models for most components used in the design. However, this introduced software package can help researchers and designers to model a solar battery-charging public station. Also, the visibility study for this station does not included her because of several reasons such as the cost of the PV panel is decreased with time and construction cost with other power electronic components differ from place to another in the world.

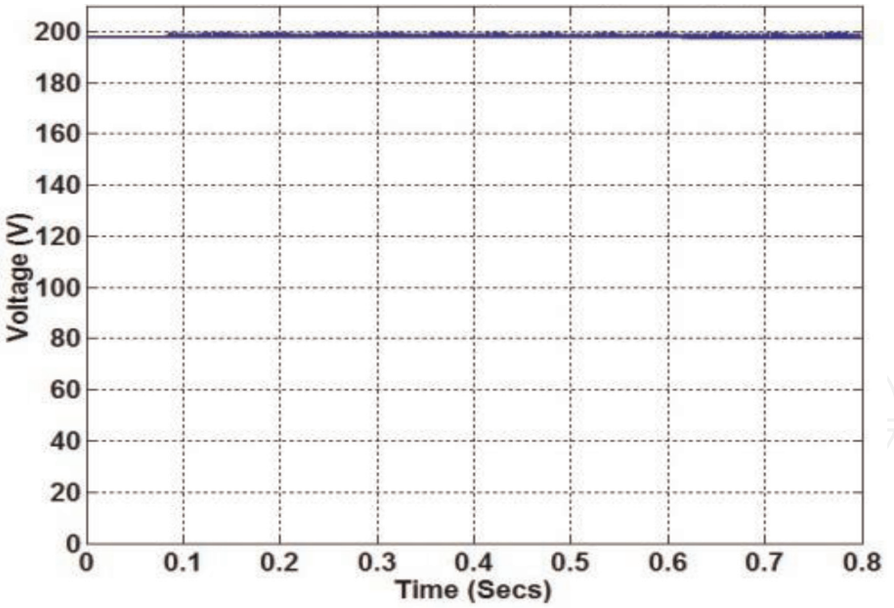

Figure 21.
Battery-terminal voltage profile through charging.

6. Summary and recommendations

The chapter of this book puts in the hands of the reader the main tools required to model and design a solar public station for EV-battery charging. This station is energized from the on-grid PV system and proposed as an off-board 100 kW rating. The proposed system includes a sophisticated un-plugged technique to overcome the problems of wiring and hazards. This technique depends on the inductively coupled power transfer through the air-core transformer with a large air gap. Two main parts are implied and classified according to the winding of the transformer: primary and secondary parts. The primary part is placed on the floor of the station, and the other part is installed at the bottom of the car. A Matlab/Simulink with m-file is powerful tool that used to model and simulate all components such as PV model, maximum power point tracking (MPPT) technique, boost inverter, three-level inverter, series-series (SS) compensation with high-frequency resonant converter, air-core transformer, rectifier, switched-mode power converter, and battery-charging smart controller. The proposed station is tested by charging four 19-kW batteries for EV from Honda Company. Simulation results include the battery state of charge (SOC), charging voltage, and currents. Using high-frequency compensation with switched-mode power converter and smart PI-tuning controller for the charger make the charging process is so fast. The ideal overall efficiency for the proposed solar station is relatively high due to assuming ideal cases for all modeled components. Finally, due to the rapid change in the cost of all components, especially the PV panels, this chapter does not imply a visible study for the station. So, it is preferable to conduct a visible study for each country separately.

Author details

Essamudin Ali Ebrahim
Power Electronics and Energy Conversion Department, Electronics Research Institute, Cairo, Egypt

*Address all correspondence to: essamudin@eri.sci.eg; essamudin@yahoo.com

References

[1] Ebrahim EA. A general software package for modelling a contact-less electric-vehicles battery-charging public-station fed from on-grid photo-voltaic array. Elsevier Journal of Electrical Systems and Information Technology. 2018;**5**:271-286. DOI: 10.1016/j.jesit.2018.04.001

[2] Wang C-S, Stielau OH, Covic GA. Design considerations for a contactless electric vehicle battery charger. IEEE Transactions on Industrial Electronics. 2005;**52**(5):1308-1314. DOI: 10.1109/TIE.2005.855672

[3] Sallán J, Villa JL, Llombart A, Fco J. Sanz: Optimal design of ICPT systems applied to electric vehicle battery charge. IEEE Transactions on Industrial Electronics. 2009;**56**(6):2140-2149. DOI: 10.1109/TIE.2009.2015359

[4] Villa JL, Sallán J, Llombart A, Fco Sanz J. Design of a high frequency inductively coupled power transfer system for electric vehicle battery charge. Elsevier Journal of Applied Energy. 2009;**86**:355-363. DOI: 10.1016/j.apenergy.2008.05.009

[5] Tabari M, Yazdani A. Stability of a dc distribution system for power system integration of plug-In hybrid electric vehicles. IEEE Transactions on Smart Grid. 2014;**5**(5):2464-2674. DOI: 10.1109/TSG.2014.2331558

[6] Kim S, Kang F-S. Multifunctional on-board battery charger for plug-in electric vehicles. IEEE Transactions on Industrial Electronics. 2015;**62**(6): 3460-3472. DOI: 10.1109/TIE.2014.2376878

[7] Janghorban S, Teixeira C, Holmes DG, McGoldrick P, Yu X. Magnetics design for a 2.5-kW battery charger. In: Proceedings of Australasian Universities Power Engineering Conference, AUPEC 2014, Curtin University, Perth, Australia. 2014. pp. 1-6

[8] Ebrahim EA. A novel approach of bacteria-foraging optimized controller for DC motor and centrifugal pump set fed from photo-voltaic Array. Journal of Next Generation Information Technology. 2015;**6**(1):21-31

[9] Miskovski D, Williamson SS. Modelling and simulation of a photovoltaic (PV) based inductive power transfer electric vehicle public charging station. In: Proceedings of IEEE Transportation & Electrification Conference and Expo (ITEC 2013). 2013. pp. 1-6. DOI: 10.1109/ITEC.2013.6573491

[10] Halder T. Charge controller of solar photo-voltaic panel fed (SPV) battery. In: Proceedings of India Inter. Conf. on Power Electronics (IICPE), New Delhi, India. 2011. pp. 1-4. DOI: 10.1109/IICPE.2011.5728056

[11] Robalino DM et al. Design of a docking station for solar charged electric and fuel cell vehicles. In: Proceedings of 2009 International Conference on Clean Electrical Power, Capri. 2009. pp. 655-660

[12] Giroux P, Sybille G, Osorio C, Chandrachood S. Grid-Connected PV Array. USA: Research Centre Press, Mathwork Co.; 2012

[13] Mathwork Corporation: Matlab/Simulink 2012b, User's Guide. USA; 2012

[14] Available from: http://www.solardesigntool.com/components/module-panel-olar/Sunpower/514/SPR-305-WHT-U/specification-data-sheet.html

[15] Esram T, Chapman PL. Comparison of photovoltaic array maximum power point tracking techniques. IEEE

Transactions on Energy Conversion. 2007;**22**(2):439-449. DOI: 10.1109/TEC.2006.874230

[16] Harrabi N, Soussi M, Aitouche A. Maximum power control for photovoltaic power based on fuzzy Takagi-Sugeno model. Journal of Electrical Engineering. 2015;**25**:1-11

[17] Pouresmaeil E, Miracle DM, Bellmunt OG. Control scheme of three-level NPC inverter for integration of renewable energy resources into AC grid. IEEE Systems Journal. 2012;**6**(2): 242-253

[18] Subsingha W. Design and analysis three phase three level diode-clamped grid connected inverter. Energy Procedia. 2016;**89**:130-136

[19] Powerex Company Catalogue: Application Notes to Three-Level Inverter Technology, First Release; 2009:1-12

[20] Tremblay O, Dessaint L-A. Experimental validation of a battery dynamic model for EV applications. World Electric Vehicle Journal. 2009;**3**

[21] El Shahat A, Haddad R, Kalaani Y. Lead acid battery modeling for photo-voltaic applications. Journal of Electrical Engineering. 2015;**15**